Computer Simulations of Canada's RADARSAT2 GMTI

Shen Chiu and Chuck Livingstone
Space Systems and Technology Section, Defence Research Establishment Ottawa
3701 Carling Avenue, Ottawa, Ontario, Canada K1A 0Z4

Tony Knight and Ishuwa Sikaneta
MacDonald, Dettwiler and Associates Ltd.
13800 Commerce Parkway, Richmond, B.C., Canada V6V 2J3

Abstract

Canada's RADARSAT2 commercial SAR satellite will have an experimental operating mode that will allow ground moving target indication (GMTI) measurements to be made with received data. This mode is also called MODEX (Moving Object Detection Experiment). In the GMTI or MODEX mode of operation, the spacecraft's radar antenna is partitioned into two apertures that sequentially observe the scene of interest from the same points in space. Data is simultaneously and coherently received from both apertures and is down-linked in parallel channels for processing to extract moving target radial speeds in their SAR image context. This paper provides an analysis of SAR-GMTI performance based on computer modeling and simulations. Two SAR-MTI processing approaches are being explored. One utilizes the classical DPCA clutter cancellation technique to provide sub-clutter visibility for dim slowly moving targets. The other is based on the along-track (temporal) SAR interferometer technique, where amplitude and phase information of the slow-moving targets are exploited to extract them from the dominant clutter background. Performances of the two approaches are compared.

1.0 Introduction

A space based radar (SBR), operating at 800 km altitude, has an orbital speed of approximately 7.5 km/s. Under the RADARSAT2 antenna design constraints (this is a synthetic aperture radar satellite), acceptable range and azimuth ambiguity levels can be achieved for the two GMTI apertures at pulse repetition frequencies (PRFs) in the vicinity of 2000 Hz, for terrain grazing angles between 80^0 and 40^0. The radar design allows PRFs up to 3800 Hz to be selected by accepting ambiguity level and swath width trade-offs. The available PRF and grazing angle ranges result in the majority of the received signal spectrum being occupied by strong clutter returns from the "stationary" terrain. Since the radar is fundamentally a SAR, there is no azimuth beam steering capability that would allow the radar beam to dwell on a point on the earth's surface more than the synthetic aperture time. Single channel GMTI measurements, based on the extraction of the target Doppler spectrum are severely constrained to large cross section, rapidly moving targets whose motion has a large radial component.

The detection probability and the estimation accuracy can be increased considerably by use of multiple aperture antennas. Space-time adaptive processing (STAP) techniques can be used to provide sub-clutter visibility for dim slowly moving targets. The displaced phase center antenna (DPCA) technique, which is a form of STAP, is well suited for SBR. This technique requires at least two antenna phase centers be arranged along the flight direction, each with its own dedicated receiver channel. The phase centers of the two sub-apertures are displaced physically in such a way that a pair of pulses from the two receivers appear to be generated from a stationary radar when an appropriate sampling rate (i.e. the PRF) is chosen. Since the clutter Doppler frequency from a stationary radar is concentrated at dc, a conventional MTI canceller can be used to null the background clutter. This is the classical DPCA two phase center clutter suppression technique. In this approach, the received signals from channels 1 and 2 are time shifted to register them spatially, then subtracted to cancel the background clutter. Target enhancement is limited by the noise floor and phase noise of the radar, by scene phase noise and by target fading.

This paper reports on a preliminary investigation of the GMTI performance of two SAR-MTI processors developed by the authors for RADARSAT2. The two SAR-MTI processing architectures are introduced in Sec. 2.0. This is followed by a discussion of the newly proposed RADARSAT2 GMTI mode in Sec. 3.0, including its sensor configuration and parameters. Sec. 4.0 looks at the SBR MTI simulation tool used to simulate realistic radar signals and Sec. 5.0 defines the experimental scenario to be used for this study. Simulation results are then presented in Sec. 6.0, This is followed by a discussion of some experimental airborne data and GMTI results in Sec. 7.0. The two GMTI approaches are then analyzed and compared in Sec. 8.0. Finally, Sec. 9.0 provides some conclusions. The results presented in this paper are based on the analysis of a single case.

2.0 MTI Processors

Three types of MTI processing are being considered for RADARSAT2 MODEX mode: SAR displaced phase center antenna (DPCA) processing, along-track interferometry (ATI), and space-time adaptive processing (STAP). In this investigation we will only consider the first two processors.

Paper presented at the RTO SET Symposium on "Space-Based Observation Technology", held on the Island of Samos, Greece, 16-18 October 2000, and published in RTO MP-61.

The proposed GMTI processors for RADARSAT2 MODEX are shown in Fig. 1. The first MTI processor, which we shall call the SAR/DPCA processor, is the limiting case of the two-beam DPCA clutter canceller. The pulses from the leading antenna are delayed by T, the integral pulse number needed to effectuate the DPCA condition. SAR processing is then performed on each channel. The outputs of the SAR modules are subsequently subtracted to yield a GMTI image. The stationary clutter signals are suppressed, and only signals from moving targets with sufficient radial velocity remain.

In true classical DPCA, target detection would be performed on the raw difference data. Performance may be improved by taking advantage of the SAR capability of the system and performing SAR processing on the difference data prior to detection. Due to theoretically perfect clutter cancellation of DPCA, any remaining targets in the image will correspond to moving targets. Since SAR processing is a linear operation, the SAR processing on the difference data is equivalent to performing SAR processing on the two apertures separately, and then taking their difference. The utilization of the SAR/DPCA technique to provide SAR and MTI simultaneously has also been discussed by other authors [1, 2].

In a similar way to classical DPCA, ATI uses two-displaced phase centers aligned along-track. Instead of taking the difference of the two channels, the interferometric phase is computed. This is done, as in other types of interferometry, by generating SAR images for each channel separately, and then estimating the interferometric phase by computing the phase (i.e., the complex argument) of the product of one image with the complex conjugate of the other (see Fig. 1b). The remaining phase is zero for stationary objects and non-zero otherwise. The application of the ATI technique to GMTI have also been discussed by other investigators [3, 4].

3.0 RADARSAT2 GMTI

At present time, no spaceborne radar system has a GMTI capability. Although all of the processes needed for full function GMTI have been developed for airborne systems, differences in platform velocity, range to target, and accessible depression angles between airborne and spaceborne radars result in several unknown parameters for the optimization of spaceborne GMTI sensors. Cost, complexity, available technology, and design risk have all combined to preclude the construction and launch of a full-function space-based GMTI radar.

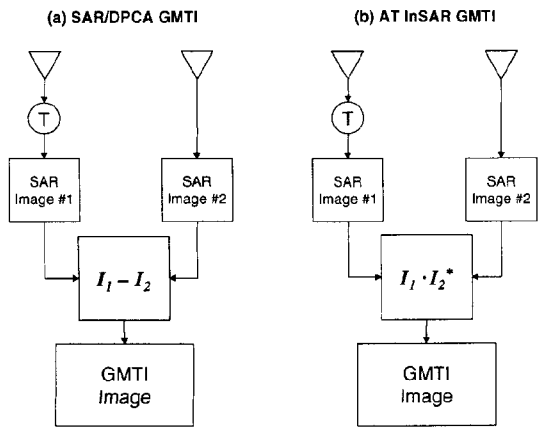

Fig. 1 Two simple SAR-MTI processors: (a) SAR/DPCA GMTI and (b) Along-Track InSAR GMTI.

When the detailed properties of GMTI and SAR systems are examined, a restricted set of GMTI functions can be added as operating modes to an appropriately designed SAR with little impact on the radar design. The RADARSAT2 MODEX is thus the world's first attempt to implement such a limited-function GMTI aboard a commercial SAR satellite. Although the subset of possible GMTI operating modes available from a radar of this type is small, such a radar could be used to validate GMTI parameters and algorithms needed for more sophisticated radars.

RADARSAT2 is currently under development and is scheduled for launch in early 2003. Preliminary information on the RADARSAT2 MODEX configuration can be found in references [5, 6]. Table 1 lists some of the SAR-MTI sensor characteristics and design parameters.

Table 1: RADARSAT2 SAR-MTI Parameters

Parameter	Value
Orbit Description:	
Type	Circular
Inclination	98.6°
AltitudeA	800 km
Active Array:	
Length x Width	15 m × 1.5 m
Number of sub-apertures	2
Orientation	Long-axis forward, Elevation boresight ±29.5° (selectable)
Look Geometry:	
Nominal Incidence Angle	10° to 60°
Search Type	Strip-map
Swath Size	150 km to 25 km
Azimuth Beam Width	Programmable from 0.21° to 0.63°
Detection Cell Size	Programmable from 25m×25m to 3m×3m
Waveform:	
Band	5.405 GHz
Bandwidth	10 to 100 MHz
Peak Power	2.4 kW (42 μs pulse) 3.7 kW (21 μs pulse)
Duty Ratio	10 %
PRF	1300 to 3800 Hz
Burst Length	up to 500 ms
Receiver Noise Temperature:	695 K

Detection cell sizes are based on RADARSAT2's standard beams and the new ultrafine beam that operates at 100 MHz bandwidth to produce 3m×3m image resolution cells. The RADARSAT2 antenna looks broadside to track. While this limits the capability to dwell on an area of interest for theater defence applications, it should be well-suited as an experimental SAR-GMTI sensor, providing very useful real data.

The proposed "dual-receive" mode uses the full antenna on transmit, while the antenna is divided into forward and aft apertures on receive. The one-way phase center separation can be controlled by the number of columns used for receiving, but have a nominal value of 7.5 m. An "alternating-transmit mode" has also been considered, where pulses would be alternately transmitted from each aperture of the antenna. This mode would give a larger two-way phase center separation than the dual-receive mode. However, only the first "dual-receive" mode will be considered in this study.

4.0 SBR MTI Simulator

The simulation results described in the next section were obtained using a sophisticated space-based MTI radar simulator known as the SBRMTISIM, developed by Sicom Systems Ltd. for DND. The simulator provides an Environment Window showing a world map overlaid with the satellite ground track. The user can specify the look-geometry and define clutter regions and targets to create a scenario (see Fig. 2). Clutter is modeled as a set of regularly distributed scatterers with user specified cross-section, statistics and internal motion, and targets are modeled as point scatterers with user specified cross-section and fading statistics. Other windows are used to specify the radar and antenna parameters, and other parameters needed to characterize the system. Once the parameters are specified, the simulator generates high-fidelity, complex baseband signals representing the received signals for the SBR. The complete, two-way path of the signal is modeled from the transmitter, to the earth, and back to the receivers.

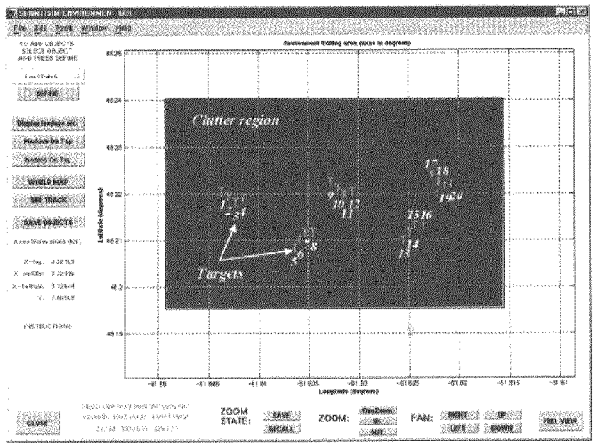

Fig. 2 SBRMTISIM Environment Window

The simulator then passes the generated data to a customized, built-in processing module, in which the architecture and algorithms are specified by the user. One of the processor options is the SAR/DPCA architecture as illustrated in Fig. 1a. The ATI processor option (Fig. 1b) has also been implemented, and a constant false-alarm rate (CFAR) detector suitable for the ATI processed signal output is currently under development. Some preliminary results are presented in Sec. 6.0.

5.0 Experimental Definition

One of RADARSAT2's beams known as a Wide Mode Beam provides swaths in the 120 km to 170 km range with multi-look ground image resolutions of about 25 m × 25 m. This mode is expected to be useful for GMTI surveillance for large strong targets [5]. In this paper, only the wide-mode beam is investigated for predicting the GMTI performance of RADARSAT2.

A carefully designed scene is created using the Environment Window (Fig. 2). A range swath of 1500 m was generated, which contains a 2.5 km × 5.0 m land-clutter patch with a reflectivity of −10 dB m^2/m^2 and a spectral width of 0.1 m/s. The clutter amplitudes are Rayleigh distributed. The same target and clutter scenario is used for both SAR/DPCA and ATI processing architectures.

A total of 20 targets occupy the clutter region (Fig. 2), with key target parameters summarized in Table 2. The targets cover a typical range of radial speeds and target radar cross-sections.

Table 2: Target Parameters

Target Number	RCS (m^2)	Speed (m/s)
1	45	15 (east)
2	45	10 (east)
3	45	5 (east)
4	45	3 (east)
5	40	15 (west)
6	40	10 (west)
7	40	5 (west)
8	40	3 (west)
9	35	15 (east)
10	35	10 (east)
11	35	5 (east)
12	35	3 (east)
13	30	15 (west)
14	30	10 (west)
15	30	5 (west)
16	30	3 (west)
17	20	15 (east)
18	20	10 (east)
19	20	5 (east)
20	20	3 (east)

The satellite heading is approximately north with the right-looking geometry. The targets are heading either east or west; as a result, the moving targets have significant radial components toward or away from radar.

A waveform with a PRF of 1988 Hz is used, which provides the necessary DPCA condition for clutter cancellation. This PRF generates 750 ms of data for each of the two 7.5 m receive sub-apertures.

6.0 Simulation Results

The first test case is one where the 20 moving targets were present with both the land clutter and the thermal noise removed from the scene. The generated raw signal data were put through the SAR/DPCA processor and the targets were detected using a cell-averaging CFAR detector to produce a MTI image as shown in Fig. 3. As expected, the MTI image is very clean with no noise- or clutter-contributed false alarms. All 20 targets were detected irrespective of their RCS or speed. The positions of these targets were shifted in azimuth according to their respective radial speed. The targets-only MTI image serves as the reference for the subsequent full scenario simulation.

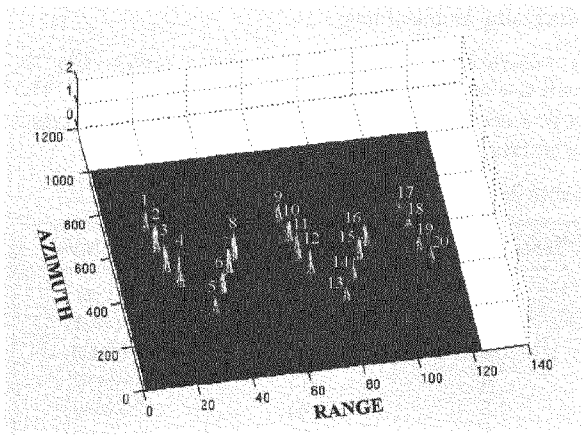

Fig. 3 MTI image of 20 moving targets without the land clutter and the thermal noise.

Next, a scenario with targets, clutter and thermal noise signals were generated. Each channel's signal data were SAR-processed separately to produce two SAR images. Fig. 4 shows the SAR image from channel 1. Most targets are below the background clutter, and no moving targets are detectable. This is expected since the brightest target in the scene has a signal-to-clutter ratio (SCR) of only about 1.2 dB. Plotting the same SAR signal in the complex plane as shown in Fig. 5, one sees that the targets are completely buried in this clutter "noise ball," making the target detection virtually impossible.

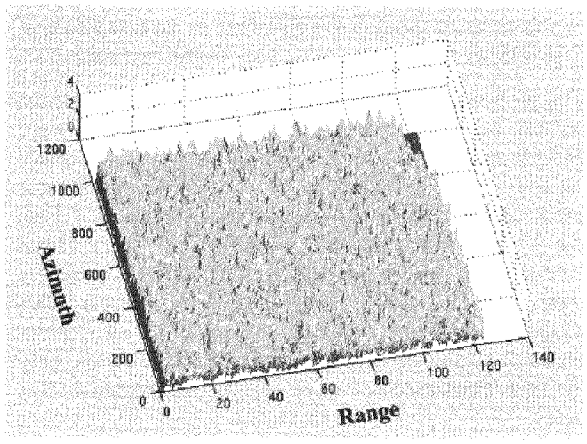

Fig. 4 Signals from channel 1 after SAR processing.

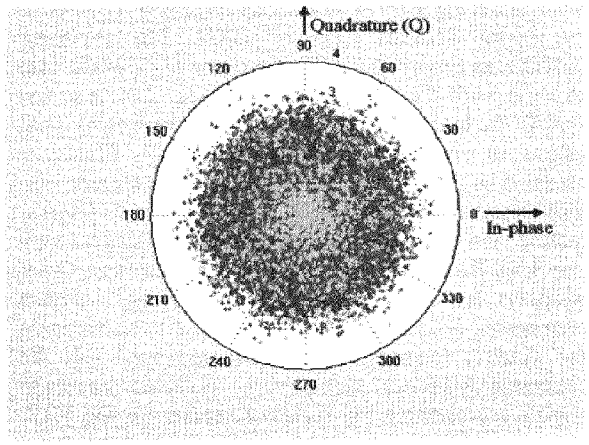

Fig. 5 Complex-plane plot of Channel 1 SAR signal.

Continuing with the signal processing chain, as depicted in Fig. 1a, the SAR signal of channel 1 is time shifted by an inter-pulse period T and then subtracted from channel 2 to produce a MTI image. As can be seen in Fig. 6, the stationary clutter signals are suppressed or whitened, leaving only the signals from the moving targets and the noise floor. The I-Q plot of the SAR/DPCA output signal is also shown in Fig. 7. The coherent clutter signal is clearly suppressed with most of the targets above the noise level.

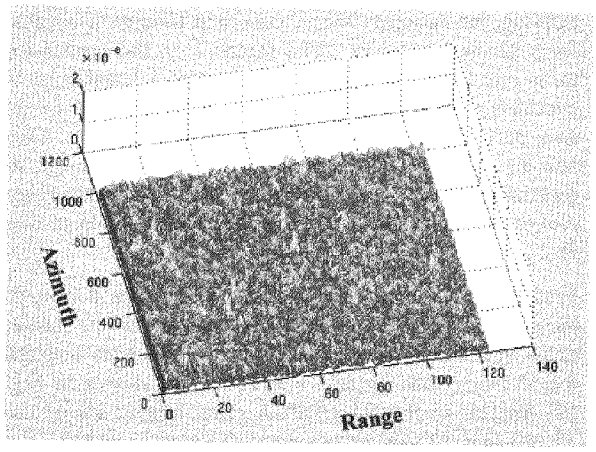

Fig. 6 Output signal from the SAR/DPCA processor, with clutter signal reduced to the noise level and some moving target signals clearly visible.

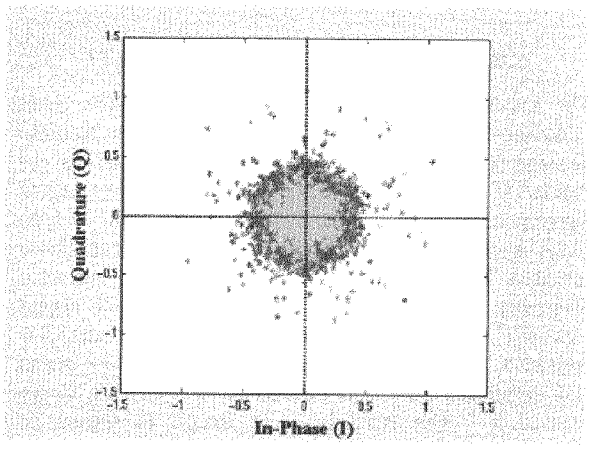

Fig. 7 I-Q complex plane plot of SAR/DPCA output signal. Dots lying outside the noise "ball" are the moving target signals.

Putting the SAR/DPCA signal through a CFAR detector, one obtains a MTI plot as shown in Fig. 8. In this case, almost all of the 15 m/s and 10 m/s targets were detected except for the 20 m^2 RCS target #17. However, all the 3 m/s targets were missed and only two of the five 5 m/s targets were detected. This is expected since the magnitude of the SAR/DPCA output signal or the "difference vector" is of the form $\sin(x/2)$, where x is directly proportional to the target radial velocity. Thus, slow-moving targets are attenuated or suppressed along with the stationary clutter. In this test, three of the four 20 m^2 targets were missed, indicating that long integration times provided by SAR are necessary for smaller targets and that MTI is also needed if reliable detection is to be achieved in clutter.

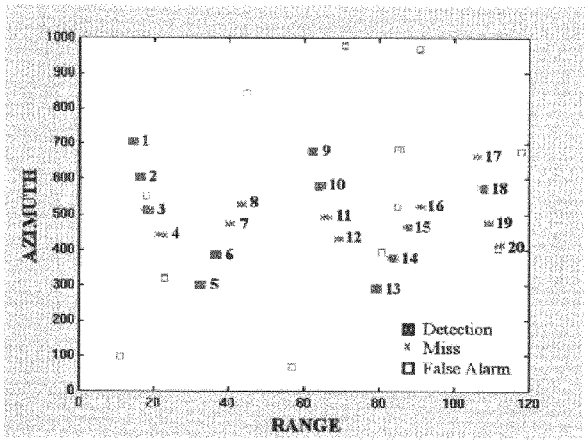

Fig. 8 Output of CFAR detector.

With the ATI processing architecture (Fig. 1b) the SAR signal from channel 1 is time shifted by an inter-pulse period T and then multiplied with the conjugate of the SAR signal of channel 2 to produce an interferometric SAR image. The I-Q plot of this ATI image signal is shown in Fig. 9. The clutter-signal phase is "cancelled" giving a mean zero phase. The phase spread of the main lobe clutter around the x-axis (or in-phase axis) is due to the thermal noise, the phase noise, and other noises of the system. Moving targets with finite radial velocities appear in the figure as vectors with non-zero phases. It is clear from the plot that those moving target vectors that reside outside the main clutter region can be detected using a suitably devised detection scheme. Here we would like to suggest a simple method based on empirically fitting a set of I-Q points derived from Q-component distributions of the signal data.

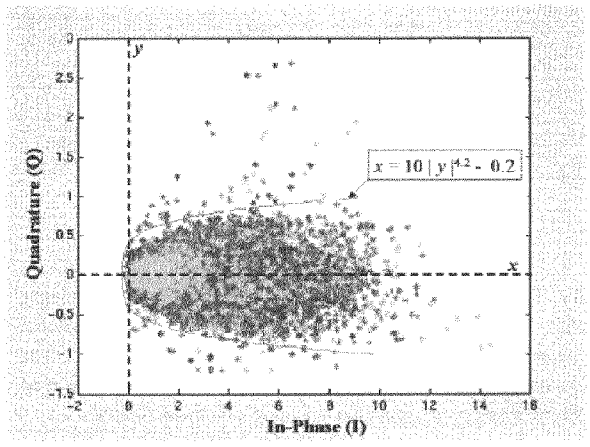

Fig. 9 Output signal from ATI processor, with clutter phases center around zero and moving target phases at non-zero values.

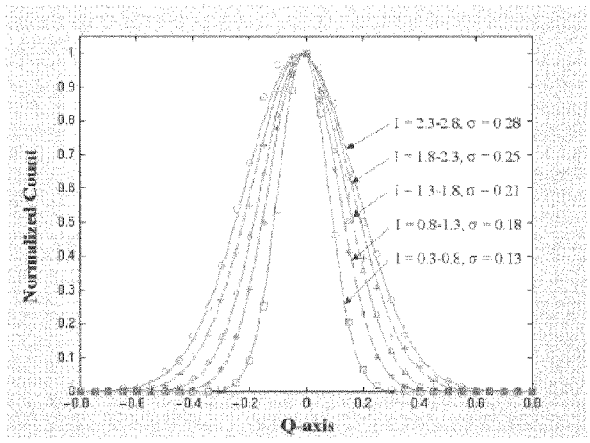

Fig. 10 Q-component distributions at different I-component range intervals.

We first proceed by dividing the x-axis into equally spaced segments and then plot the Q-component distribution of each of these segments as shown in Fig. 11. We found that the Q-component of the clutter has a Gaussian distribution. This may be expected since if the thermal noise is dominant noise component contributing to the main lobe clutter scatter and since the thermal noise is normally distributed in magnitude, we would expect also a normally distributed Q-component.

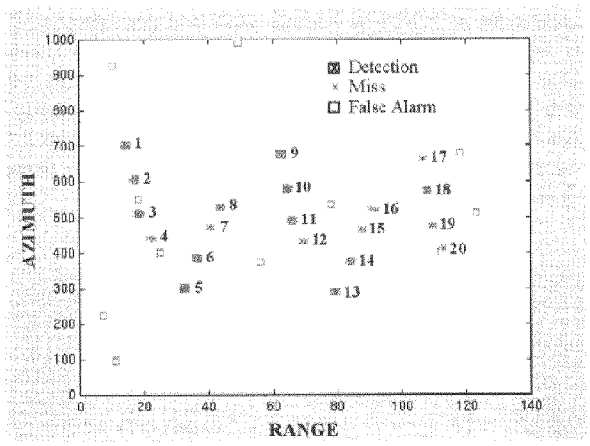

Fig. 11 Output of "$10 \cdot |y|^{4.2} - 0.2$" detector

By fitting these normally distributed Q-components with best normal curves and deriving their statistical parameters, we can then calculate the y (or Q-component) values for each of the x segments based on the desired probability of false alarm as follows:

$$P_{FA} = \frac{2 \cdot \int_{y=y_0}^{y=+\infty} e^{-\frac{y^2}{\sigma^2}} dy}{\int_{y=-\infty}^{y=+\infty} e^{-\frac{y^2}{\sigma^2}} dy}$$

Solving the equation for y_o one then obtains a y-value for a given x segment . The factor 2 on the numerator takes into account the fact that the normal distribution is symmetric. The above procedure yields a set of (x, y) data points to which one can fit a $x = F(y)$ curve. This best-fit curve is the detector that can be used to discriminate the moving targets from the stationary clutter and that will yield the specified false alarm rate P_{FA}.

Proceeding with curving fitting, one obtains a best-fit curve "$10 \cdot |y|^{4.2} - 0.2$" as the detector for the target extraction (see Fig. 9). Putting the ATI signal through this detector, one obtains a MTI plot as shown in Fig. 11. Similar to the SAR/DPCA case, almost all of the 15 m/s and 10 m/s targets were detected except for the 20 m^2 RCS target #17. All the 3 m/s targets were missed except for target #8 and only two of the five 5 m/s targets were detected. All of the 20 m^2 RCS targets were missed except for target #18, suggesting that detection is noise- limited.

7.0 Comparison of SAR/DPCA and ATI

The C-band airborne along-track interferometric SAR (Convair-580) operated by Canada Center for Remote Sensing (CCRS) was used to produce GMTI results for validation of the simulations. Two control targets moving on railway tracks at speeds of about 2.5 to 6 m/s were use in this set of experiments. The airborne raw data was processed using a modified ATI software originally developed by CCRS. The ATI output signal was put through a simple phase-amplitude detector similar to the one described above, with separate phase and amplitude detection thresholds, for moving target extraction. The resulting ATI image is shown in Fig. 12. As can be seen, the two control targets in the scene were both detected. They are also displaced in azimuth. A few vehicles on a highway and roads were also detected, also displaced in azimuth from their true positions on the highway or the roads.

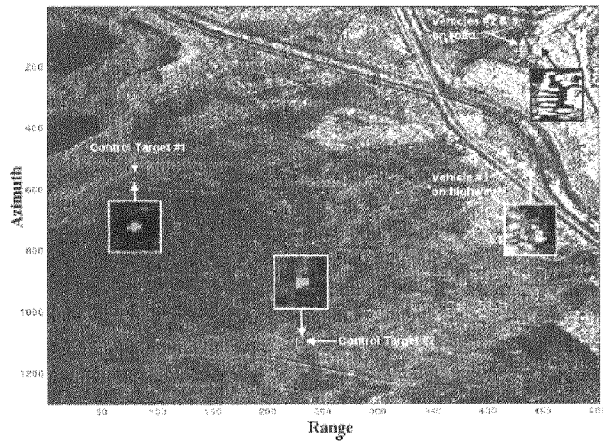

Fig. 12 ATI image showing moving targets being detected using a simple phase amplitude threshold detector.

The ATI output signal is plotted in a I-Q plot in Fig. 13. The phase-amplitude threshold detector, which has a key-hole shape in the complex signal plane, is also shown. This detector allows a moving target with phase and amplitude above certain threshold values to be declared as a detection. The amplitude threshold is necessary to minimize the noise contribution to false alarms. In this case, the two control moving targets in the scene are outside the main clutter region and are easily detected using this simple "key-hole" detection technique.

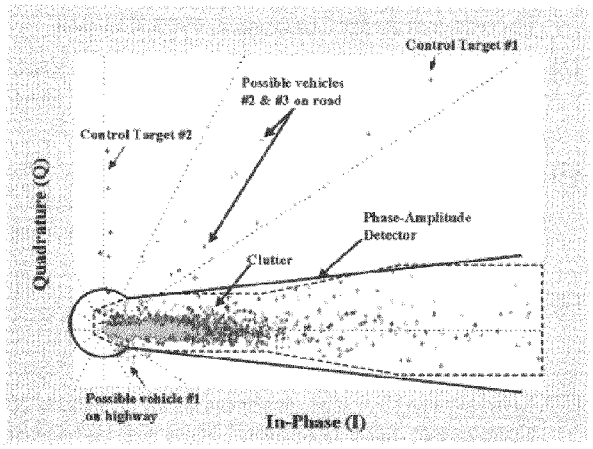

Fig. 13 Output signal from the ATI processor plotted on I-Q plane. Also shown is a simple phase-amplitude detector for moving target extraction.

The Q-component of this ATI airborne data was also found to have a Gaussian distribution as was found in the simulated data. Thus, a more sophisticated and optimized detector can be similarly constructed using the procedure described in the previous section to ensure that smaller, slower targets are not excluded from the detection region (i.e., outside the "key-hole" area).

8.0 Comparison of SAR/DPCA and ATI

At first, ATI would appear to have an advantage over SAR/DPCA in that the ideal PRF is no longer required. The two-antenna SAR/DPCA suffers the shortcoming of any two-pulse delay-line canceller in that its output signal is equal to the difference of two slightly different signal vectors and its magnitude is related to the target radial velocity as follows:

$$a = |\mathbf{S}_1 - \mathbf{S}_2| = |S(x,y)|\left|1 - e^{j4\pi(R_2 - R_1)/\lambda}\right|$$

which simplifies to:

$$a = 2 \cdot \left|\sin\left(\frac{2\pi(R_2 - R_1)}{\lambda}\right)\right| \cdot |S(x,y)|$$

$$= 2 \cdot \left|\sin\left(2\pi \frac{V_r \delta t}{\lambda}\right)\right| \cdot |S(x,y)| \quad ,$$

where R_1 and R_2 are ranges from the forward and aftward phase centers, respectively, to the moving target, and V_r is the target radial velocity. δt is the "DPCA time," which in this case is equal to the pulse repetition interval (PRI). Thus, slow-moving targets are significantly attenuated by the DPCA clutter rejection filter.

On the other hand, the ATI output is the signal power (as opposed to the signal voltage from the SAR/DPCA processor) and its magnitude is simply equal to $|S(x,y)|^2$. The targets are not suppressed along with the stationary clutter when one utilizes phase and amplitude information for target. Careful examination of the ATI processor shows that the ATI phase depends on the signal-to-clutter ratio (SCR). For example, in a 25 m × 25 m resolution cell, target and clutter signal vectors will be added within the cell. Ignoring noise, the output image from the first channel can be written as

$$S_1 = V_{s,1} + V_c \,,$$

where V_c is the clutter and $V_{s,1}$ is the signal from the target of interest in channel 1. Similarly, for channel 2 we can write

$$S_2 = V_{s,2} + V_c \,.$$

The estimated phase from the ATI processor output is

$$\text{Arctan}(S_1 \cdot S_2^*) \,.$$

But the correct interferometric phase for the signal of interest is

$$\text{Arctan}(V_{s,1} \cdot V_{s,2}^*) \,.$$

The estimated phase is "attenuated" by the clutter contained in the same resolution cell as the target. The smaller the SCR, the more likely the target will become buried within the main clutter region in the complex plane and less likely be extracted from the clutter. As illustrated in Fig. 12, the resulting signal vector within a resolution cell has a phase angle that is consistently smaller than the actual moving target's signal phase. For a clutter vector that is of same size as that of the target vector, the resulting signal vector would have a phase value that is exactly half of that of the moving target. The effect will be most severe for low SCR targets. This is indeed observed for targets 17 to 20, where only target 18 has a confirmed detection. However, the clutter contamination effect can be mitigated by selecting radar resolution cell areas that are closer to the physical size of the target. For RADARSAT2 MODEX studies, cell sizes of 6 m × 6 m and smaller may be needed to extract weak targets.

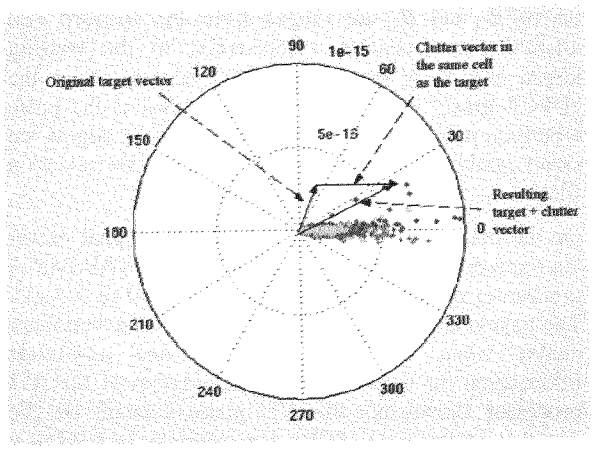

Fig. 14 The target signal phase within a resolution cell is being "attenuated" the clutter signal occupying the same cell.

In ATI processing, noise tends to scatter the clutter signal around zero phase and may obscure the nearby targets with smaller phase angles. High system noise could potentially present a problem for detecting bright but slow moving targets. However, the overall performance of ATI processor was shown to be about the same as that of the SAR/DPCA approach for the target and clutter parameters examined.

On the other hand, both ATI and SAR/DPCA suffer from the limited efficiency of the two-pulse canceller: to get high sensitivity, the two antennas have to be widely separated, but this leads to a comb of blind velocities $v_{blind} = kv_p\lambda/d$, where k is an integer, v_p is the platform velocity, and d is the antenna separation.

9.0 Conclusions

At first, it was expected that ATI would outperform classical DPCA when the SCR is high and that DPCA would be superior when the SCR is low. But this expectation does not appear to be supported by the present study. The two processor architectures both appear to perform well under the target and clutter parameters examined. Both approaches have difficulty detecting targets with radial speed below 5 m/s or RCS smaller than 20 m^2. The initial simulations and airborne ATI results here are encouraging, and suggest that detection of ground moving targets of sufficient radar cross section is possible with a sensor of the RADARSAT2 GMTI class. Further studies are expected to refine these performance data and characterize the full range of a space-based GMTI capability.

Acknowledgement

Special thanks to Dr. David Liang for his valuable advice and for his encouragement throughout this work and to Georgio Dinardo for his computer support. This work is carried out by the DREO Space Systems Group.

References

[1] Coe, D.J., White, R.G., " Moving Target Detection in SAR Imagery: Experimental Results," IEEE International Radar Conference, 1995, 644-649.

[2] Stockburger, E.F., Held, D.N., "Interferometric Moving Ground Target Imaging," IEEE International Radar Conference, 1995, 438-443.

[3] Ender, J.H.G., "Space-Time Processing for Multichannel Synthetic Aperture Radar," Electronics & Communication Engineering Journal, 11, 1999, 29-38.

[4] Yadin, E., "Evaluation of Noise and Clutter Induced Relocation Error in SAR MTI," IEEE International Radar Conference, 1995, 650-655.

[5] Livingstone, C., "The Addition of MTI Modes to Commercial SAR Satellites," Proc. Of 10th CASI Conference on Astronautics, Ottawa, Canada, October 26-28, 1998.

[6] Luscombe, A., "The Radarsat Project," IEEE Canadian Review, Fall 1995.